SUPPLEMENTAL METHODS

Cell lines

Human myeloma cell lines (MM.1S, AMO-1, INA-6) were obtained from ATCC or DSMZ, authenticated by STR analysis, and routinely tested for mycoplasma. They were cultured in RPMI 1640 medium supplemented with 20% FBS, GlutaMAX™, and 100 U/mL penicillin-streptomycin. The murine Vκ*MYC myeloma cell line (Vκ32245) was kindly provided by Drs. Marta Chesi (Mayo Clinic, Scottdale, AZ) and maintained in the same medium. The murine NK cell line KILC.2 (Kerafast®) was cultured in IMDM supplemented with 30% FBS, GlutaMAX, penicillin-streptomycin, and β-mercaptoethanol, with added murine SCF (50 ng/mL, Peprotech, 250-03) and IL-7 (25 ng/mL, Peprotech, 217-17). For cytotoxicity assays, KILC.2 cells were pre-activated with murine IL-2 (20 ng/mL, Peprotech, 212-12) for 24 hours prior to co-culture.

Flow Cytometry

Cells were resuspended in FACS buffer (D-PBS containing 2% FBS) and stained with fluorescently conjugated antibodies for 20–40 minutes at 4 °C. After staining, cells were washed twice and resuspended in fresh FACS buffer. Samples were acquired on a CytoFLEX (Beckman Coulter), or Cytoflex Flow Cytometer (Beckman Coulter, Beckman Coulter Navios Flow Cytometer) or FACSAria-Fusion or FACSAria III flow cytometer (BD Biosciences). Data were analyzed using FlowJo software (version 10.10.0). Fluorescence compensation was performed using UltraComp eBeads™ (Invitrogen, Cat. #01-2222-42). For murine samples analysis, gating strategy used was FSC-A/SSC-A for lymphocyte population, single cells gated in SSC-A/SSC-H and then NK cell population was gated on murine CD3-/NK1.1+/NKp46 to determine IFN-γ, CD107a, CD69, CD48 and CD244 expression.

Molecular Cloning and DNA Plasmids

Gene fragments encoding murine CD48 (mature and immature isoforms; UniProt P18181), and dCas9-KRAB with a BFP2-mTag reporter were synthesized by Twist Bioscience (South San Francisco, CA).

Constructs were assembled into lentiviral expression vectors using Gibson assembly (NEB, E2611S) and verified by plasmid sequencing (Plasmidsaurus, South San Francisco, CA). Plasmids were amplified in *E. coli* NEB 5-alpha Competent Cells (High Efficiency; NEB, C2987H) and Stbl3 Competent Cells (Macro Lab, UC Berkeley, CA). DNA was purified using either the QIAprep Spin Miniprep Kit (Qiagen, 27104) or the Plasmid Plus Midi Kit (Qiagen).

Lentiviral Vector Production

Lenti-X 293T cells (Takara, Cat. #632180) were transfected with plasmids encoding murine CD48, firefly luciferase–mCherry, or dCas9–BFP2-mTag using the TransIT™-Lenti Transfection Reagent (Mirus Bio, Cat. #MIR6600), according to the manufacturer's instructions. Cells were cultured for 2–3 days post-transfection, and lentiviral supernatants were collected at 48 and 72 hours. Viral particles were concentrated using Lenti-X Concentrator (Takara Bio, Cat. #631232) following the manufacturer's protocol.

In vitro cytotoxicity assays

The Vκ*MYC cell line (Vκ32245) was stably transduced with luciferase and engineered to express various CD48 densities. For cytotoxicity assays, 50,000 tumor cells were seeded in IMDM-cell media in white 96-well plates (Greiner Bio-One), followed by co-culture with pre-activated KILC.2 cells at varying effector-to-target (E:T) ratios (30:1 to 1:10) in IMDM, with triplicate wells per condition. After 18–24 hours of incubation at 37 °C, D-luciferin (375 µg/mL, Gold Biotechnology, LUCK-1G) was added, and luminescence was measured using a GloMax Explorer (Promega). Bioluminescence signals were averaged across replicates and normalized within each condition to generate a 0–100% cytotoxicity scale.

Murine blood NK cell detection

Peripheral blood was collected via submandibular vein puncture using sterile lancets. Samples were obtained weekly during the first four weeks after initiation of the NK-cell depletion protocol and every other week thereafter. Peripheral blood was collected from all mice in each experimental group at each time point unless otherwise indicated. Red blood cells were lysed using ammonium chloride lysis buffer (ACK buffer),

and the remaining leukocytes were washed and resuspended in D-PBS supplemented with 2% FBS prior to flow cytometric analysis. NK cells were identified using antibodies against murine CD3, NK1.1, and NKp46. All samples were analyzed on a CytoFLEX flow cytometer (Beckman Coulter) as described above.

Plate-Bound Stimulation Assay for Murine NK Cells

To evaluate NK cell activation via receptor engagement(1), 96-well high-binding plates (Corning Costar Brand 96-Well EIA/RIA Plates, Cat: 07200721) were coated overnight at 4°C or 2 hr at 37ºC with PBS-diluted antibodies (typically 25 µg/mL; e.g., anti-NK1.1 [PK136]). Control wells contained PBS or PMA/ionomycin. After washing, single-cell suspensions from murine spleen and bone marrow were added without prior NK enrichment (0.5–1 × 10^6 cells/well in complete media). Anti-CD107a and monensin were added, and cells were incubated for 6 hours at 37°C. Post-stimulation, cells were stained for viability, NK markers (NK1.1, NKp46, CD3ε), and intracellular IFN-γ. Flow cytometry was used to assess degranulation (CD107a) and cytokine production.

CRISPR-Cas9 Gene Knockouts

Cas9 protein and either target-specific or scrambled sgRNA (Synthego, Redwood City, CA) were complexed at a 1:2.5 molar ratio and incubated at 37 °C for 10–15 minutes. A total of 1 × 10^6 Vκ*MYC, AMO1, or KILC.2 cells were washed with PBS and resuspended in 20 µL of nucleofection solution containing the Cas9–sgRNA complex. KILC.2 cells were electroporated using the P3 Primary Cell 4D-Nucleofector™ X Kit S and program CM-137; Vκ*MYC and AMO1 cells were electroporated using the SF Cell Line 4D-Nucleofector™ X Kit S and program DS-137 (Lonza). Immediately post-nucleofection, cells were plated into 80 µL of pre-warmed IMDM or RPMI 1640 media, incubated at 37 °C for 15 minutes, and then transferred to complete recovery media. CD48-negative clones were identified by flow cytometry and sorted using a FACSAria Fusion or FACSAria III (BD Biosciences). Human and murine sgRNA sequences used were taken from Brunello and Brie Library respectively(2): Human: TFAP2A: AUCCUCGCAGGGACUACAGG, ESRRA: AGACACCAGTGCATTCACTG, CD48: ATGTACAGTG CGCCACTCTG, MEF2B: CCTCTTCCAGTATGCCAGCA, CD74: AGCCGC GGAGCCCTGTACAC, TCGCGCTGGTCATCCATGAC, RELA: ACTACGACCTGAATGCTGTG. Murine: Cd48:

GAACGAGUUGAAGAUAACCC, Inpp5d (SHIP1): CAUCCGAAGGUGUCCCCAUG (sgRNA sequence from Synthego tool). Scrambled sgRNA: non-targeting control specified by Synthego.

Genomic DNA confirmation of CRISPR-Cas9 knockouts:

Genomic DNA was extracted from 1 × 10^6 Vk*MYC or KILC.2 cells (fresh or frozen) using the Monarch® Genomic DNA Purification Kit (NEB, Cat. #T3010S). Primers were designed using the IDT PrimerQuest™ Tool (Integrated DNA Technologies, Coralville, IA) to generate ~500 bp amplicons, with at least 200 bp flanking each side of the sgRNA target site. Primers were reconstituted in nuclease-free water to a final concentration of 10 µM. PCR amplification was performed using NEBNext® High-Fidelity 2X PCR Master Mix (NEB, Cat. #M0541S) with 0.5 µM of each primer and 1 ng to 1 µg of genomic DNA. PCR products were purified using the QIAquick PCR Purification Kit (QIAGEN, Cat. #28104) and submitted for Sanger sequencing (Quintara Biosciences, Fort Collins, CO). Resulting .ab1 files were analyzed using the ICE (Inference of CRISPR Edits) tool from Synthego (https://ice.synthego.com), and indel percentage, model fit (R^2), and knockout score were used to evaluate editing efficiency. Primer sequences: m*INPP5D (SHIP1).* Set 1: Forward: GGATGTGAGGCGTGAGTG, Reverse: GAAAGCATCCTTCAACCTCCA. Set 2: Forward: ATACTTCTATTTGCACCTTTGC, Reverse: CCTCCAAAGAGGTACTCTAGTC. Set 3: Forward: TTTGCAAAGGGCTCCTG, Reverse: TAGTCTAGAAGCACCCGTGA. m*CD48.* Set 1: Forward: GGACCCACTTGGACCATATAAA, Reverse: TAGGTCAGGCTCACTCTCAA. Set 2: Forward: GGCAGCAATGTAACCCTGAA, Reverse: GCAGCAGCTATCAGCTTTGA. Set 3: Forward: CCACCGGCAGCAATGTA, Reverse: GCTTTGATATCTGGTAGGTCAGG. MEF2B: Set 1: Forward: CATGTTCGAGGAAGGGTTAGG, Reverse: AGCCACAAAGCCAGATGAA; Set 2: Forward: TTACCAGCTCAGCCAGAAAG, Reverse: CAGCAGAAATAAAGCACGTCAG. CD244: Set 1: Forward: TCAGCTTGGGTTCTCTTTCC, Reverse: ATAGGACACATTGCCATCCC; Set 2: Forward: TGACCATGTGGTTAGCATCTC, Reverse: TGTACCAAGCATAGGACACATT. ESRRA: Set 1: Forward: CTCACAGCCTGTCCACAAA, Reverse: GACCACAATCTCTCGGTCAAA; Set 2: Forward: CTGGGAACAGGGACGATTT, Reverse: CAAAGAGGTCACAGAGGGTAG. TFAP2A: Set1: Forward: CCACCCTACCAGCCTATCT, Reverse: ACTCTCCGCCTCCGAATAA, Set 2: Forward: CCCAATGCCGACTTCCA, Reverse: CTGTATGTTCCAGGTATCCTTTCT. RELA: Set 1:

Forward: CCATTCAGTACTCTCCCACTTTAC, Reverse: GGGCAGAGAAGAGTAGACAAATAC; Set 2: Forward: ACATGACATTCAGGCCACAG, Reverse: GCTGGGCAGAGAAGAGTAGA.

CRISPRi sgRNA Cloning and Lentiviral Transduction for a Doxycycline inducible Knock-down system in Vk*MYC

To generate sgRNA-expressing constructs for CRISPR interference (CRISPRi), we used the FgH1tUTG lentiviral vector (Addgene #70183), which harbors an H1 promoter with a Tet-inducible sgRNA cassette(3). Guide sequences (~20 bp) were selected from the Weissman lab CRISPRi-v2 library(4) and modified with 4-bp overhangs (5′-TCCC for the forward strand and 5′-AAAC for the reverse complement) to allow directional cloning into the BsmBI-v2-digested FgH1tUTG backbone. The vector was linearized by overnight digestion with BsmBI-v2 at 55°C, followed by gel purification. Forward and reverse oligos were annealed in T4 ligase buffer by heating to 95°C for 2 minutes and slowly cooled to room temperature. Annealed oligos were diluted (1:100 final) and ligated into the dephosphorylated backbone using T4 DNA ligase with a 1:20 vector-to-insert molar ratio, as calculated via the NEBioCalculator. Ligation reactions were incubated at 16°C overnight, and 1–5 µL of the ligation product was transformed into competent *E. coli*. Lentiviral particles were produced and used to transduce dCas9-KRAB-BFP2mTag Vκ*MYC (Cas9-KRAB–expressing). Transduced cells were sorted based on fluorescent reporters (e.g., BFP and GFP) for downstream phenotypic or functional assays. For treatment of Vκ*MYC cells to induce expression of the sgRNA, doxycycline hyclate(Sigma-Aldrich D9891) was dissolved in sterile water at a stock concentration of 50 mg/ml and added to tissue culture medium for a final concentration of 1 µg/ml for 48-72 hours, before phenotypic confirmation by flow cytometry. Oligos used to clone sgRNA sequences used for CD138 knock down were as follows: **TCCC**GGAGACAGAGCCTAACGCAG, **AAAC**CTGCGTTAGGCTCTGTCTCC. Scramble sgRNA: **TCCC**GGGAACCACATGGAATTCGA, **AAAC**TCGAATTCCATGTGGTTCCC.

Multivariate Cox Proportional Hazards Modeling for CD48

Differential gene expression analysis based on cytogenetic risk was performed on RNAseq data from primary MM samples from the Multiple Myeloma Research Foundation (MMRF) CoMMpass study (release

IA19). Sample-level cytogenetic metadata, including translocations involving NSD2, MYC, MAF, and MAFB, and copy-number alterations del17p13, gain1q21, and del1p22, along with NK-cell cluster groups, were extracted from the provided SeqFISH files and merged by sample identifier. Samples missing any metadata or with non-intersecting identifiers were excluded. Using clinical and survival information in CoMMpass, we fit a Cox model using the survival package(5) (v3.8-3) for cytogenetic variables, and relapse status was coded as factors (levels 0/1). Hazard ratios (HRs) and 95% confidence intervals were extracted from the model summary. Statistical significance was assessed at $\alpha = 0.05$, two-sided. We visualized the multivariate HRs using the forestmodel package (v0.6.2)(6), and composed with ggplot2 (v3.5.1) with all covariates displayed on a single forest plot(7). The Cox model was fit by maximizing the partial likelihood (with Efron's method for ties), and inference was provided via the Wald test for individual coefficients and the likelihood-ratio and score (log-rank) tests for the overall model fit. Stage-stratified analyses were additionally performed separately in newly diagnosed MM (NDMM) and relapsed/refractory MM (RRMM) samples. Kaplan–Meier analyses compared the top and bottom 20% of CD48-expressing tumors and NK-ligand cluster membership within each disease stage. Separate multivariate Cox proportional hazards models were then fitted for NDMM and RRMM, including CD48 VST expression, NK-ligand cluster membership, and cytogenetic variables (NSD2/t(4;14), MYC, MAF, MAFB, del1p22, del17p13, and gain1q21).

ChIP-seq and ATAC-seq analysis

Raw ATAC-seq and H3K27Ac ChIP-seq data from MM patients and normal Memory B cells, Plasmablasts, and Plasma cells were downloaded from the European Nucleotide Archive (accession: PRJEB25605). Paired-end reads were aligned to the human reference genome (hg19) using Bowtie2. Only uniquely mapped reads with ≤2 mismatches were retained. Clonal reads, defined as reads mapping to the same genomic position and strand, were collapsed into a single representative read. Peak calling was performed using MACS2 or HOMER program. To investigate transcriptional regulation of CD48, motif enrichment analyses were conducted within ATAC-seq peaks located near the CD48 promoter. Motif predictions were generated using the PROMO tool and ENCODE transcription factor databases (V3 builds 336 and 161). Public ATAC-seq data from purified human immune-cell populations were obtained from GEO accession

GSE125164, including CD14+ monocytes, CD19+ B cells, CD4+ helper T cells, CD8+ cytotoxic T cells, and NK cells from three donors. Additional NK-cell ATAC-seq datasets were obtained from GSE89668 and GSE188031. BigWig files were downloaded from GEO and visualized at the CD48 locus in the hg19 genome assembly using the Integrative Genomics Viewer (IGV). Public ChIP-seq datasets for MEF2B, MEF2C, RELA, TFAP2A, and ESRRA were obtained from GEO and the ENCODE Project Consortium. For ENCODE datasets, signal tracks (bigWig) and peak calls (bigBed/narrowPeak) were downloaded and visualized in IGV. ENCODE bigWig tracks represented ChIP-seq enrichment as –log10(P) relative to input, and corresponding peak files were used to annotate transcription factor binding sites. The CD48 locus was examined for transcription factor occupancy and co-binding patterns. Dataset accession numbers, cell lines, and cell-type descriptions are provided in Supplemental Table 2.

Machine learning analysis for transcriptional regulation of CD48 expression

A curated list of 89 transcription factors was generated from ATAC-seq, ChIP-seq, PROMO, and ENCODE databases for model construction. RNA-seq data (TPM values) from 776 $CD138^+$ myeloma samples in the CoMMpass MMRF dataset (release IA19) were log-transformed and used as input features. An XGBoost (Extreme Gradient Boosting) model was implemented using the *xgboost* package in Python via Google Colab A100GPU. All transcription factors co-expressed with CD48 were included as predictors. Hyperparameter optimization was performed using randomized search with 10-fold cross-validation across 5,000 iterations, exploring parameters including colsample_bytree, colsample_bylevel, colsample_bynode, gamma, learning_rate, max_depth, n_estimators, and subsample. Model interpretability was assessed using SHAP (Shapley Additive Explanations) analysis, applied to the test set (20% of data). SHAP values quantify each transcription factor's contribution to the model's predicted CD48 expression for each individual sample, with positive SHAP values indicating that higher expression of the factor predicts higher CD48 expression, and negative values indicating the opposite. Mean absolute SHAP values were used to rank transcription factors by their overall importance, and summary plots (Figure 2C) were generated to visualize these relationships, where each dot represents one patient and color indicates the relative expression of each factor (red = high, blue = low). Model performance was evaluated using R^2 and adjusted R^2 values, as well as mean absolute error across folds to ensure robustness across training/test splits. This

approach parallels our previously published analyses of transcriptional regulators for CD38, CD70, and CD46 in MM (8–10).

scRNA-seq Analysis of CD48, CD244, and NK Cell Function

Single-cell RNA sequencing data from GSE223060 (11) was analyzed using Seurat (v4.3.0) (12) in R (v4.1.2). Cells with fewer than 500 detected genes, fewer than 1,000 total RNA counts, more than 50,000 features, or >10% mitochondrial gene content were excluded. Normalization and identification of highly variable genes were performed prior to integration. Batch correction was conducted using the Harmony package (v0.1.1)(13), grouping by experimental condition. Dimensionality reduction was performed using PCA and UMAP, and graph-based clustering was performed in Seurat at a resolution of 0.5. Gene symbols were annotated using biomaRt, and cluster annotation was informed by prior publication metadata (11, 14). Visualization was performed with ggplot2(15) (v3.5.1) and gridExtra (v2.3)(16).

Validation Using Public scRNA-seq Compendium

A large public collection of scRNA-seq and scTCR-seq data from more than 200 samples from 182 patients with multiple myeloma, MGUS, and SMM, and non-cancer controls(17) (panImmune.h5ad), was accessed through Zenodo (https://zenodo.org/records/13646014). Data was primarily collected from Gene Expression Omnibus (GEO) Maura et al. under accession GSE161195(18, 19), Bailur et al. (GSE163278 (20)). Oetjen et al. (GSE120221(21)). Granja et al. (GSE139369(22)), Zavidij et al. (GSE124310(23)), Kfoury et al. (GSE143791(24)), and Zheng et al. (GSE156728(25)). Analysis was done in Python (Scanpy v1.9) via Google Colab on an A100 GPU. Sample group annotations (“HD,” “MGUS,” “SMM,” “MM”) were assigned based on regex matching of sample IDs. After QC filtering (<500 genes, <1,000 RNA counts, >10,000 features, >10% mitochondrial content), standard Scanpy normalization and log1p transformation were applied. CD48 expression was visualized using Seaborn boxplots across groups. For NK-cell analyses, cells annotated as NK cells were subset and compared across HD, MGUS, SMM, and MM disease stages. Expression of AP-1 family members was quantified across disease groups, and an exhaustion score was calculated as the mean normalized expression of LAG3, TIGIT, KLRG1, KLRC1, CISH, and PDCD1. Pairwise comparisons were performed using Mann–Whitney U tests with Benjamini–

Hochberg correction. For HD-versus-MM NK-cell subclustering, normalized NK-cell expression data were used to identify highly variable genes, followed by scaling, PCA, nearest-neighbor graph construction, UMAP, and Leiden clustering (resolution = 0.5). AP-1 family expression was subsequently compared across NK-cell subclusters and disease groups.

Cell-Cell Communication Analysis with CellChat

To explore ligand–receptor signaling in MM bone marrow, CellChat (v1.6.1) (26) was performed on a subset of 9 MM patient samples from the GSE223060 dataset that met the threshold of ≥25% plasma cells (MMRF_1325, MMRF_1505, MMRF_1537, MMRF_1640, MMRF_1720, MMRF_1967, MMRF_2038, MMRF_2251, and MMRF_2259). CellChat analysis was also performed independently for 8 HD. Data were extracted from the "data" slot of the RNA assay. Cell type labels were based on Seurat identities. Using CellChatDB.human, overexpressed genes and interactions were identified and signaling networks were inferred with communication probabilities. Networks were filtered (minimum 10 cells per group), and CD48-specific interactions were visualized using circle and chord diagrams as well as heatmaps with netVisual_aggregate() and netVisual_heatmap().

Antibodies

Marker	Fluorophore	Reactivity	Cat #	Lot #	Company
NK 1.1	APC	Anti-Mouse	156506	B348948	Biolegend
CD3	APC Fire	Anti-Mouse	100248	B314610	Biolegend
NKp46	BV421	Anti-Mouse	137612	B377892	Biolegend
CD244	PE	Anti-Mouse	133508	B399032	Biolegend
CD48	FITC	Anti-Mouse	103404	B379375	Biolegend
CD4	FITC	Anti-Mouse	100510	B334835	Biolegend
CD48	APC	Anti-Mouse	103411	B341107	Biolegend

F4/80	APC	Anti-Mouse	123116	B385351	Biolegend
I-A/I-E	FITC	Anti-Mouse	107606	B398140	Biolegend
CD48	PE	Anti-Mouse	103406	B359895	Biolegend
CD138	PE	Anti-Mouse	142504	B349831	Biolegend
CD19	APC	Anti-Mouse	BD 550992	240299	BD Biosciences
B220	APC	Anti-Mouse	103212	B37972	Biolegend
CD11b	APC	Anti-Mouse	101212	B336472	Biolegend
Ly-6G	FITC	Anti-Mouse	127606	B333904	Biolegend
CD16	PE	Anti-Mouse	158004	B333920	Biolegend
CD14	APC Fire	Anti-Mouse	123332	B314277	Biolegend
CD25	APC	Anti-Mouse	101910	B307760	Biolegend
TNF-α	PE	Anti-Mouse	506305	B395648	Biolegend
IFN-γ	PE	Anti-Mouse	505807	B396584	Biolegend
CD69	FITC	Anti-Mouse	104506	B432803	Biolegend
Granzyme B	PE	Anti-Mouse	372208	B402218	Biolegend
CD107a	PE	Anti-Mouse	121612	B357949	Biolegend
IFN-γ	BV605	Anti-Mouse	505840	B432035	Biolegend
SHIP-1	PE	Anti-Mouse	656604	B414748	Biolegend
CD11b	PE	Anti-Mouse	101207	B434580	Biolegend
CD27	FITC	Anti-Mouse	124207	B443248	Biolegend
CD48	PE	Anti-Human	336708	B428906	Biolegend
CD244 (2B4)	APC	Anti-Human	393512	B439913	Biolegend
CD74	APC	Anti-Human	326812	B435619	Biolegend

Purified antibodies and reagents for NK cell Plate-bound assay

Antibody	Clone	Cat#	Lot#	Company
Purified anti-mouse NK1.1	PK136	108702	B255763	Biolegend
Purified anti-mouse CD335 (Nkp46)	29A1.4	137602	B382435	Biolegend
Purified anti-mouse CD16	S17014E	158002	B376266	Biolegend
Purified anti-mouse CD244.2 (2B4 B6 alloantigen)	m2B4	133501	B390508	Biolegend
Purified Mouse IgG2a,k isotype Ctrl	MOPC-173	400202	B370572	Biolegend
TrueStain FcX (Anti Mouse CD16/32)	93	101320	B295040	Biolegend
Brefeldin A		420601	B406627	Biolegend
Cell Activation Cocktail (without Brefeldin A) [PMA (phorbol 12-myristate-13-acetate) and ionomycin]		423302		Biolegend
Monensin		420701	B431167	Biolegend

REFERENCES

1. Aguilar OA, et al. The CD3ζ adaptor structure determines functional differences between human and mouse CD16 Fc receptor signaling. *Journal of Experimental Medicine*. 2022;219(5). https://doi.org/10.1084/jem.20220022.

2. Sanson KR, et al. Optimized libraries for CRISPR-Cas9 genetic screens with multiple modalities. *Nat Commun*. 2018;9(1):1–15.

3. Aubrey BJ, et al. An Inducible Lentiviral Guide RNA Platform Enables the Identification of Tumor-Essential Genes and Tumor-Promoting Mutations InVivo. *Cell Rep*. 2015;10(8):1422–1432.

4. Horlbeck MA, et al. Compact and highly active next-generation libraries for CRISPR-mediated gene repression and activation. *Elife*. 2016;5. https://doi.org/10.7554/eLife.19760.

5. Terry M Therneau. A Package for Survival Analysis in R [preprint]. *R package version 38-3*. 2024.

6. Kennedy N. forestmodel: Forest Plots from Regression Models. R package version 0.6.2 [preprint]. 2020.

7. H. Wickham. *ggplot2: Elegant Graphics for Data Analysis*. New York: Springer-Verlag; 2016.

8. Kasap C, et al. Targeting high-risk multiple myeloma genotypes with optimized anti-CD70 CAR-T cells. *Blood Journal*. [published online ahead of print: May 13, 2025]. https://doi.org/10.1182/blood.2024025536.

9. Wadhwa A, et al. CD46-Targeted Theranostics for PET and 225Ac-Radiopharmaceutical Therapy of Multiple Myeloma. *Clinical Cancer Research*. 2024;30(5):1009–1021.

10. Choudhry P, et al. Functional multiomics reveals genetic and pharmacologic regulation of surface CD38 in multiple myeloma. *Blood Neoplasia*. 2024;1(3):100025.

11. Yao L, et al. Single-Cell Discovery and Multiomic Characterization of Therapeutic Targets in Multiple Myeloma. *Cancer Res*. 2023;83(8):1214–1233.

12. Stuart T, et al. Comprehensive Integration of Single-Cell Data. *Cell*. 2019;177(7):1888-1902.e21.

13. Korsunsky I, et al. Fast, sensitive and accurate integration of single-cell data with Harmony. *Nat Methods*. 2019;16(12):1289–1296.

14. Pilcher WC, et al. A single-cell atlas characterizes dysregulation of the bone marrow immune microenvironment associated with outcomes in multiple myeloma [preprint]. 2024. https://doi.org/10.1101/2024.05.15.593193.

15. Wickham H, et al. Welcome to the Tidyverse. *J Open Source Softw*. 2019;4(43):1686.

16. Auguie B and AA. gridExtra: Miscellaneous Functions for “Grid” Graphics. R Package Version 2.3. https://CRAN.R-project.org/package=gridExtra [preprint]. 2017.

17. Foster KA, et al. Tumour-intrinsic features shape T cell differentiation through precursor to symptomatic multiple myeloma. *Nat Commun*. 2026;17(1). https://doi.org/10.1038/s41467-026-68718-4.

18. Maura F, et al. Genomic and immune signatures predict clinical outcome in newly diagnosed multiple myeloma treated with immunotherapy regimens. *Nat Cancer*. 2023;4(12):1660–1674.

19. Cohen YC, et al. Identification of resistance pathways and therapeutic targets in relapsed multiple myeloma patients through single-cell sequencing. *Nat Med*. 2021;27(3):491–503.

20. Bailur JK, et al. Early alterations in stem-like/marrow-resident T cells and innate and myeloid cells in preneoplastic gammopathy. *JCI Insight*. 2019;4(11). https://doi.org/10.1172/jci.insight.127807.

21. Oetjen KA, et al. Human bone marrow assessment by single-cell RNA sequencing, mass cytometry, and flow cytometry. *JCI Insight*. 2018;3(23). https://doi.org/10.1172/jci.insight.124928.

22. Granja JM, et al. Single-cell multiomic analysis identifies regulatory programs in mixed-phenotype acute leukemia. *Nat Biotechnol*. 2019;37(12):1458–1465.

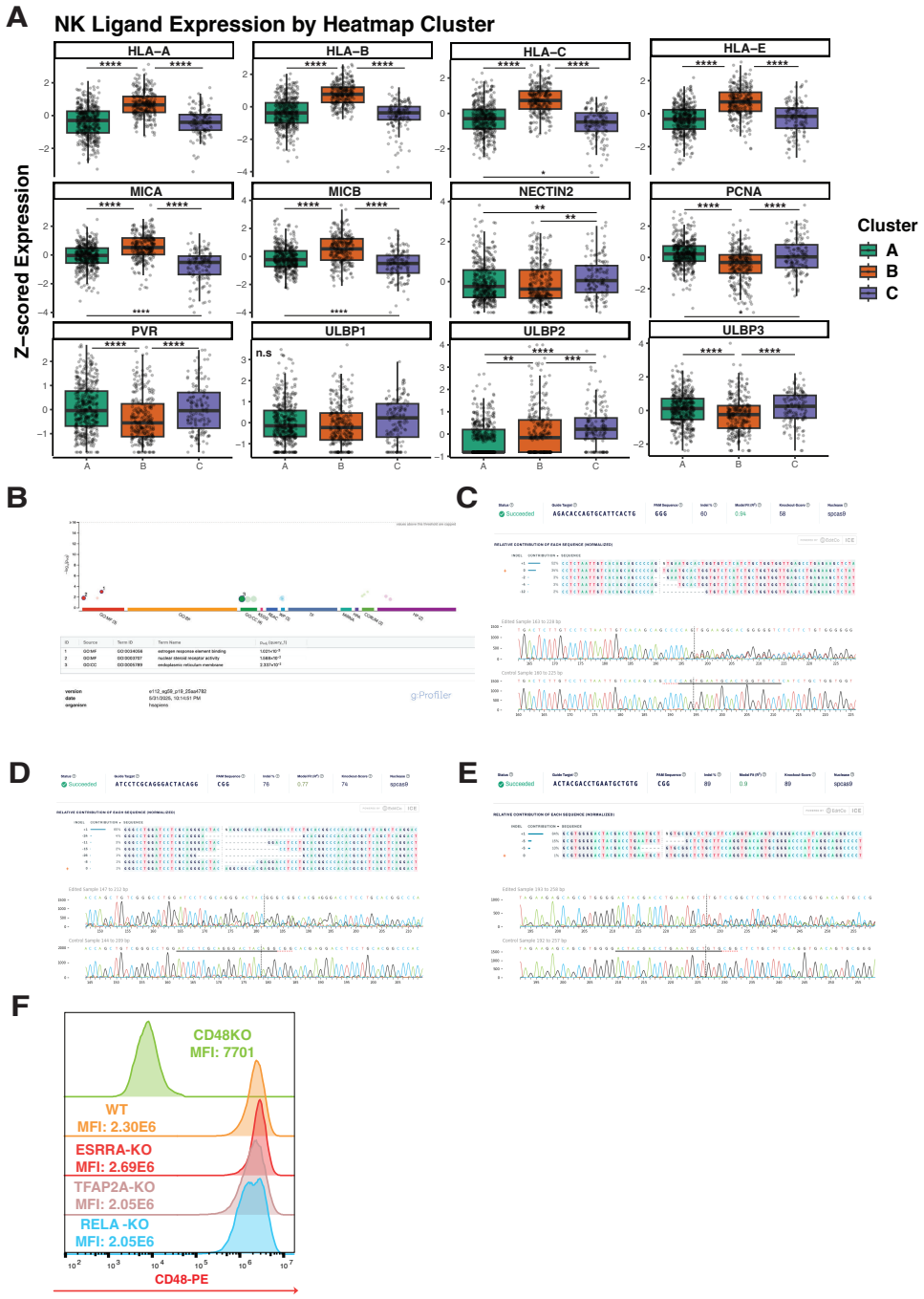
23. Zavidij O, et al. Single-cell RNA sequencing reveals compromised immune microenvironment in precursor stages of multiple myeloma. *Nat Cancer*. 2020;1(5):493–506.

24. Kfoury Y, et al. Human prostate cancer bone metastases have an actionable immunosuppressive microenvironment. *Cancer Cell*. 2021;39(11):1464-1478.e8.

25. Zheng L, et al. Pan-cancer single-cell landscape of tumor-infiltrating T cells. *Science (1979)*. 2021;374(6574). https://doi.org/10.1126/science.abe6474.

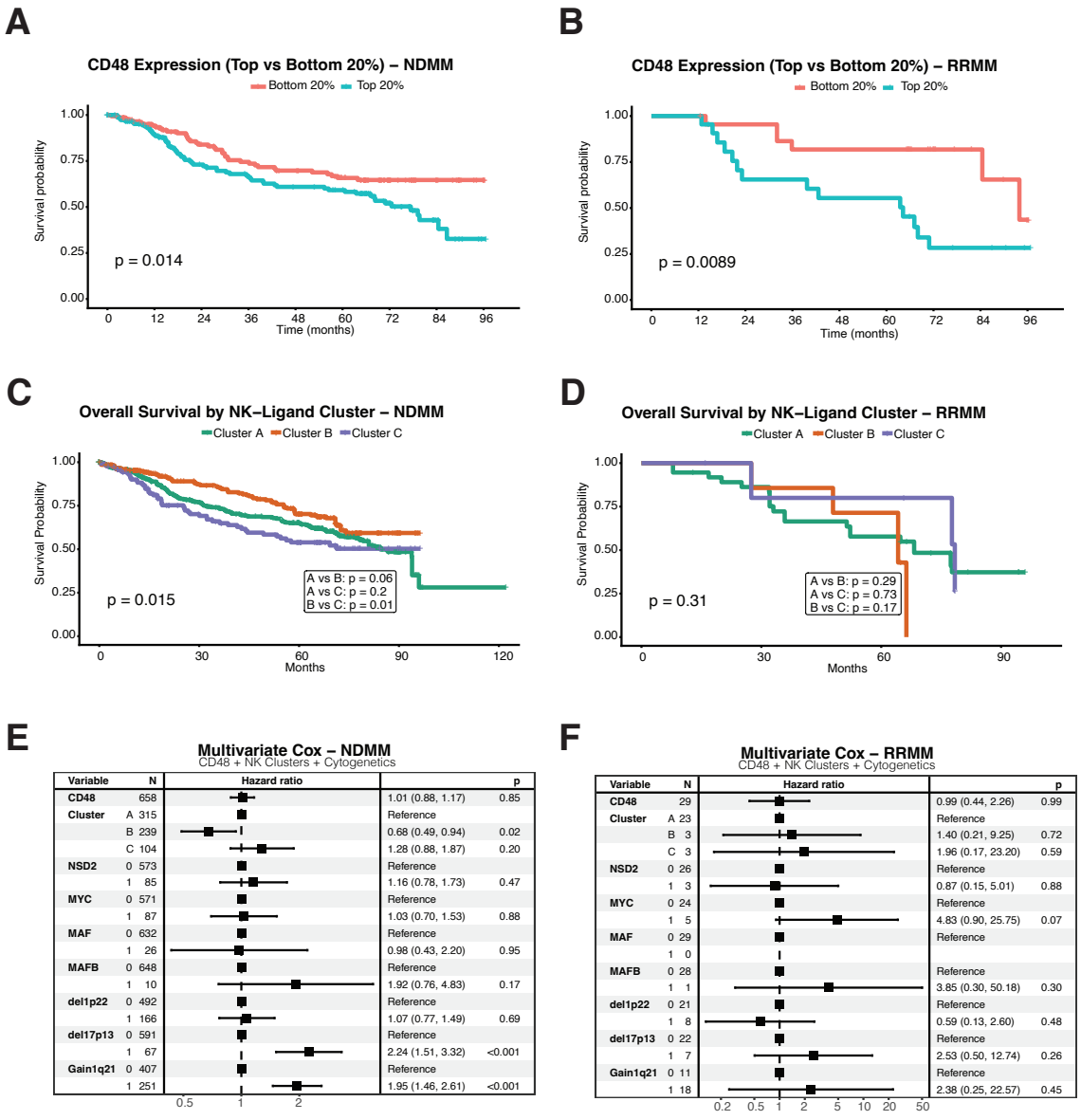
26. Jin S, et al. Inference and analysis of cell-cell communication using CellChat. *Nat Commun*. 2021;12(1). https://doi.org/10.1038/s41467-021-21246-9.

Supplementary Figure S1



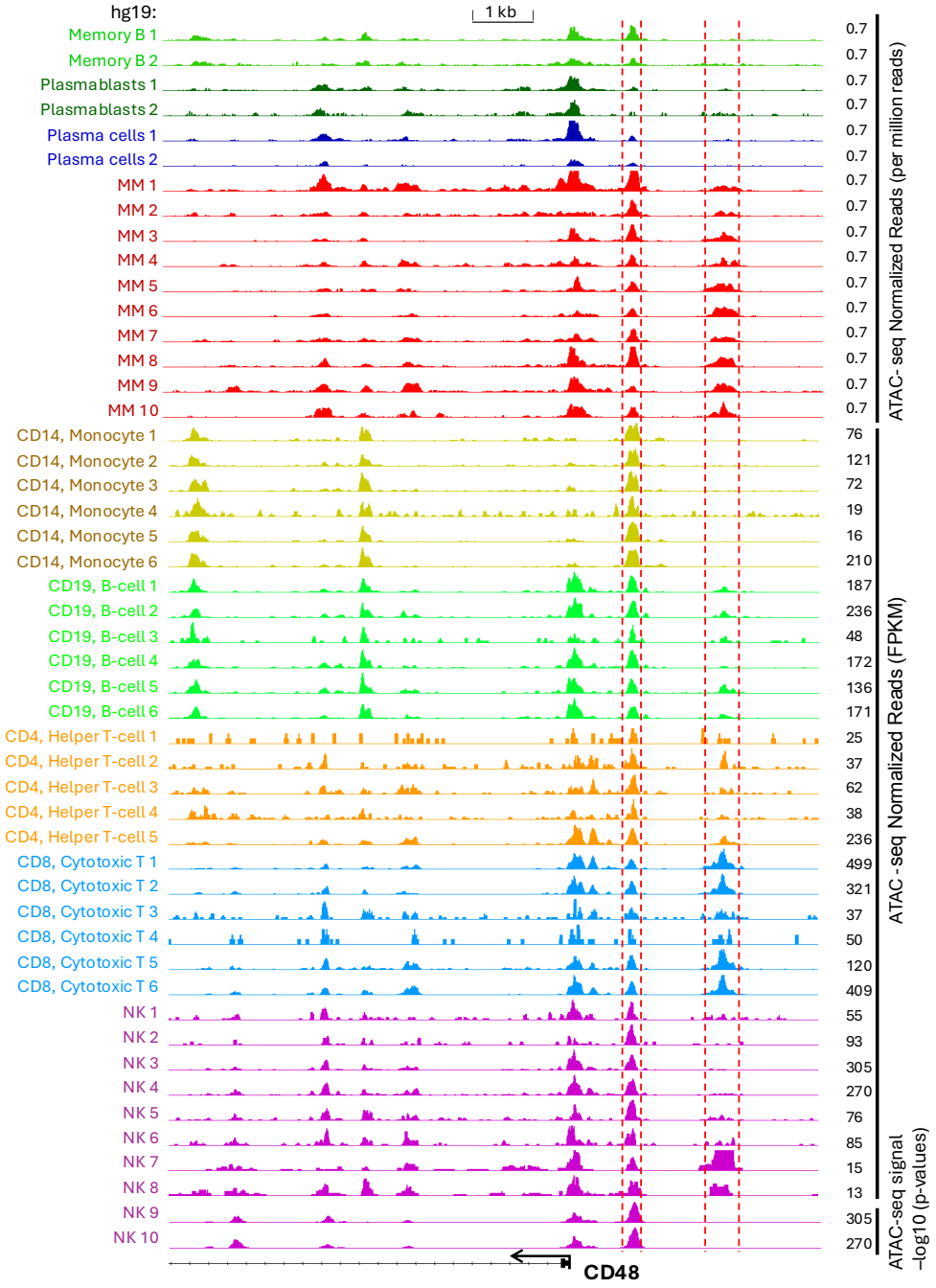
Supplemental Figure 1. NK Ligand Expression and Validation of CD48 Regulators Identified by CRISPR Screening. **A.** Boxplots showing z-scored expression of NK cell ligands in tumor cells from the CoMMpass IA19 dataset across transcriptomic clusters (A, B, C) identified by heatmap-based clustering of myeloma patient samples. Statistical significance was assessed by one-way ANOVA; ****p < 0.0001. **B.** Functional enrichment analysis using gProfiler of genes identified in genome-wide CRISPRa/KO screens as regulators of CD48 expression. **C–E.** Validation of CRISPR-mediated knockout of **C.** ESRRA, **D.** TFAP2A, **E.** RELA using Synthego ICE analysis and Sanger sequencing, showing indel spectra and editing efficiencies. **F.** Representative flow cytometry histograms of surface CD48-PE expression in AMO1 cells following knockout of the indicated genes.

Supplementary Figure S2



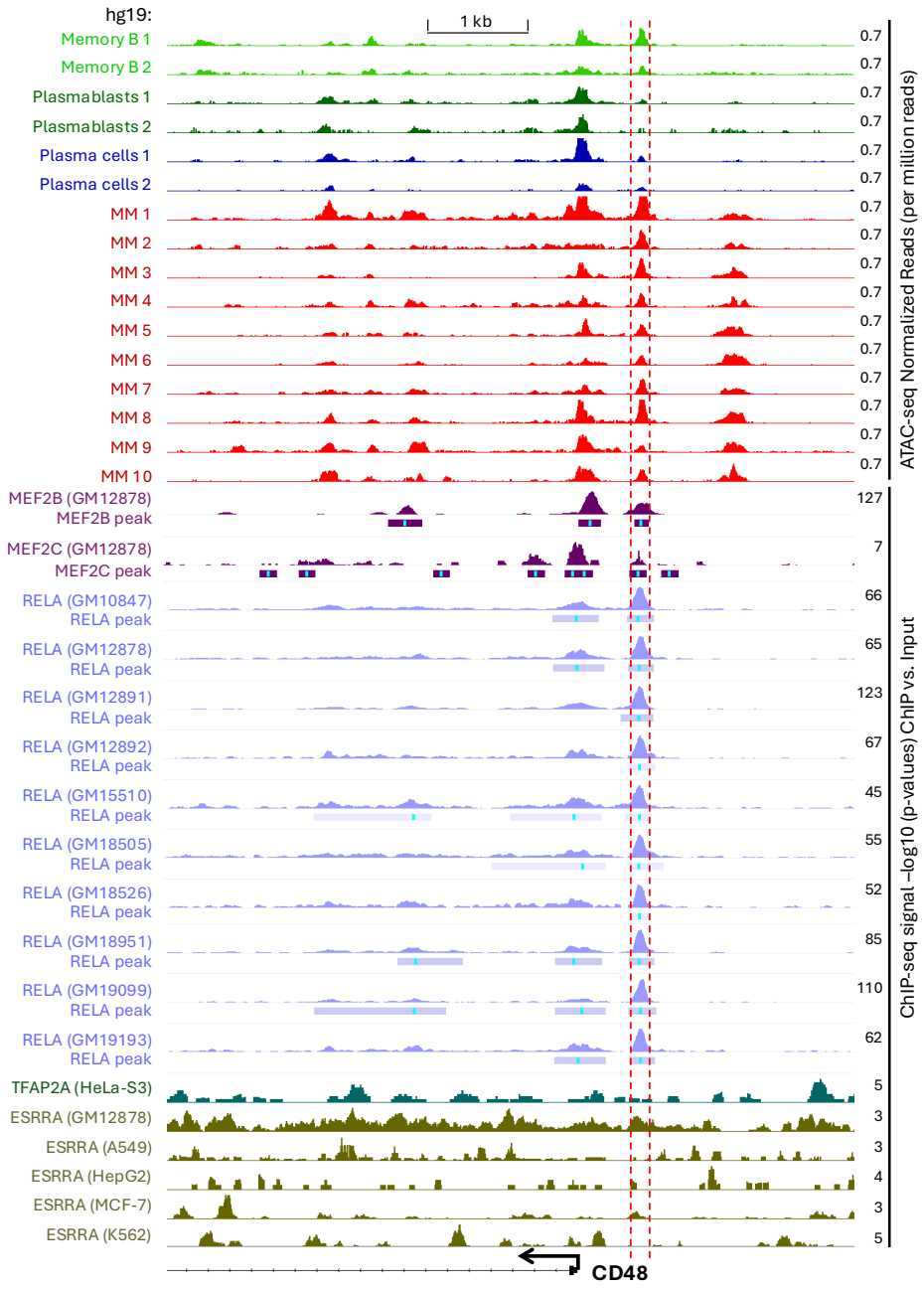
Supplemental Figure 2. **NK-ligand cluster membership and CD48 expression stratify overall survival in newly diagnosed and relapsed/refractory multiple myeloma. (A–B).** Kaplan–Meier curves of overall survival stratified by CD48 mRNA expression (top 20% vs. bottom 20%) in newly diagnosed MM (NDMM, A) and relapsed/refractory MM (RRMM, B) patients from the CoMMpass (IA19) cohort. CD48 expression was determined from CD138^{+}-enriched bulk RNA-seq.**(C–D)** Kaplan–Meier curves of overall survival by unsupervised NK-ligand cluster assignment (Clusters A, B, C; defined in Figure 1C) in NDMM (C) and RRMM (D) patients. Pairwise log-rank p-values (BH-adjusted) are shown. **(E–F)** Forest plots from multivariate Cox proportional hazards models in NDMM (E, n=658) and RRMM (F, n=29), adjusting simultaneously for CD48 VST expression, NK-ligand cluster membership, and cytogenetic risk factors (NSD2/t(4;14), MYC, MAF, MAFB, del1p22, del17p13, Gain1q21). Hazard ratios (squares) with 95% confidence intervals are shown on a logarithmic scale.

Supplementary Figure S3



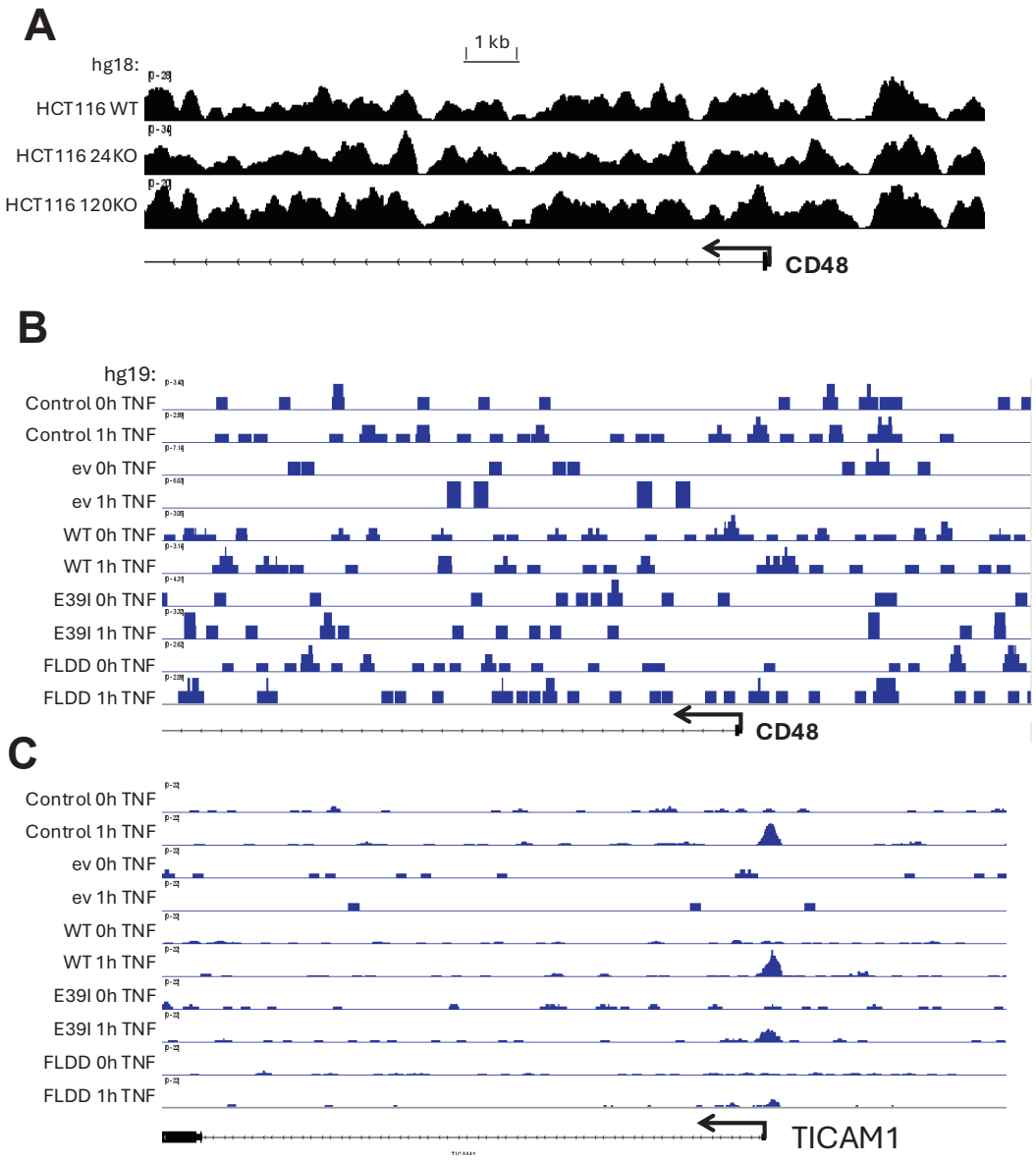
Supplemental Figure 3. ATAC-seq chromatin accessibility at the CD48 locus across hematopoietic cell types. Genome browser view (hg19) showing ATAC-seq normalized reads (per million reads) at the CD48 locus from primary MM patient samples (red, n=10) and normal memory B cells, plasmablasts, and plasma cells (top tracks), alongside publicly available ATAC-seq profiles from purified peripheral blood immune cell populations: CD14+ monocytes, CD19+ B cells, CD4+ helper T cells, CD8+ cytotoxic T cells, and NK cells. Dashed red lines demarcate the two consensus ATAC-seq peaks in the CD48 regulatory region: Peak_1 (chr1:160,682,575–160,682,845, 270 bp) and Peak_2 (chr1:160,684,020–160,684,540, 520 bp).

Supplementary Figure S4



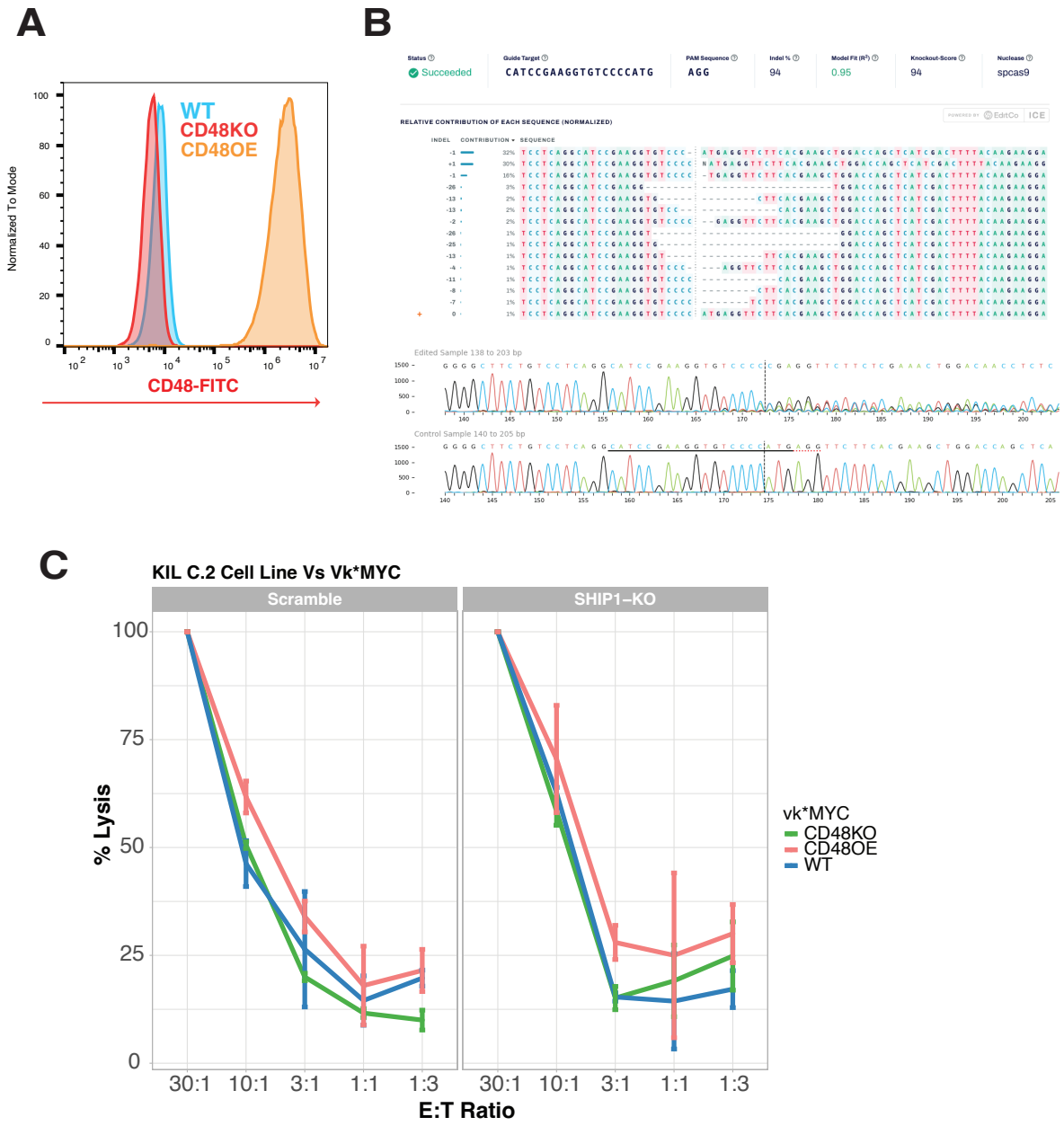
Supplemental Figure 4. ChIP-seq occupancy of predicted CD48 transcriptional regulators at the CD48 locus in B-lineage and non-hematopoietic cell types. Genome browser view showing ATAC-seq accessibility tracks from primary patient samples (top, reproduced from Figure 2A) and publicly available ChIP-seq tracks for five nominated transcription factors across multiple cell types. MEF2B (GM12878, GSE127481; purple), MEF2C (GM12878, GSE32465; purple), RELA across ten independent EBV-transformed lymphoblastoid cell lines from donors of diverse ethnic backgrounds (GSE31477; light blue), TFAP2A (HeLa-S3, GSE31477; teal), and ESRRA across five cell lines (GM12878, A549, HepG2, MCF-7, K562; olive). Dashed red vertical lines demarcate the consensus ATAC-seq peaks in the CD48 promoter region.

Supplementary Figure S5



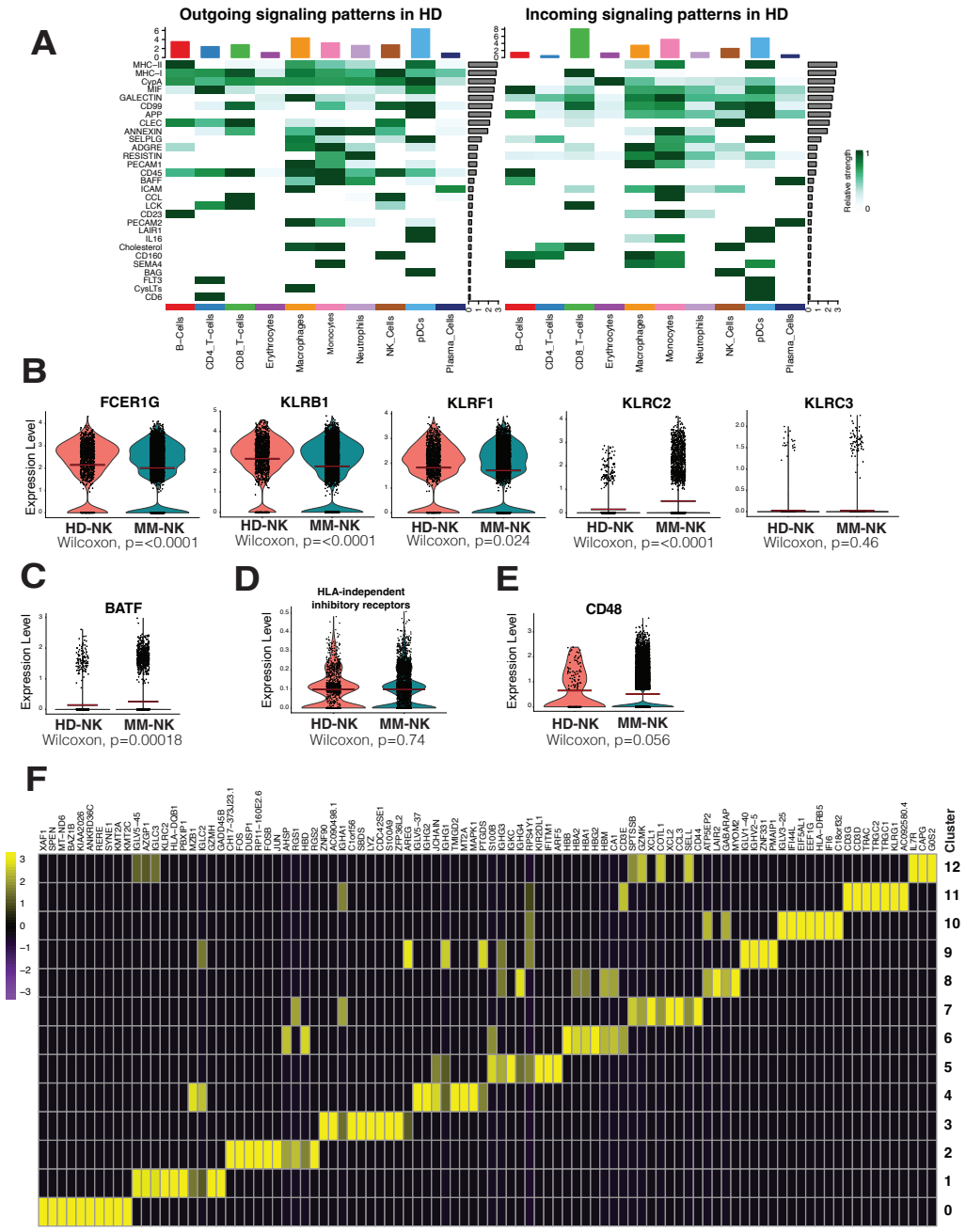
Supplemental Figure 5. Absence of TFAP2A and RELA occupancy at the CD48 locus in non-hematopoietic cell lines. A. TFAP2A ChIP-seq at the CD48 locus (hg18) in HCT116 parental (WT) and two CRISPR/Cas9 AP-2α knockout clones (24KO, 120KO; GSE155165). **B–C.** RELA ChIP-seq in HeLa cells with siRNA-mediated p65 depletion, reconstituted with wild-type (WT), DNA-binding-deficient (E39I), transactivation-deficient (FLDD) p65, or empty vector (ev), with or without TNF-α stimulation (GSE116284). **B.** No RELA enrichment is detected at the CD48 locus under any condition. **C.** At the TICAM1 locus, a canonical NF-κB target, robust p65 binding is confirmed following TNF-α stimulation, validating ChIP-seq assay quality.

Supplementary Figure S6



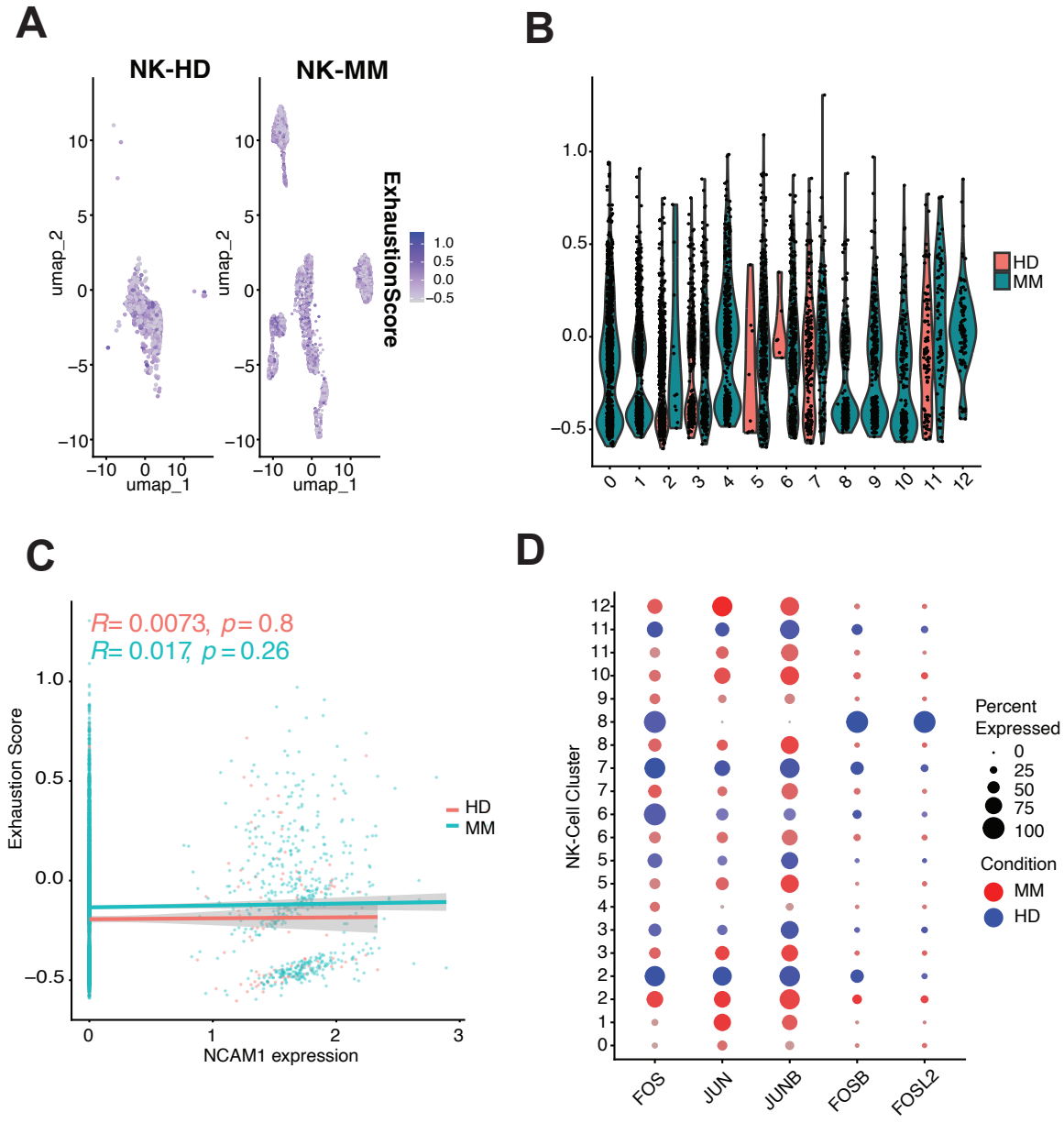
Supplemental Figure 6. Functional and Genotypic Validation of CD48 Manipulation in Murine vk*MYC Cells. **A.** Flow cytometry histogram showing surface CD48 expression in WT, CD48KO, and CD48OE vk*MYC cells. **B.** ICE analysis confirming efficient CRISPR-mediated knockout of INPP5D (SHIP1), showing indel spectrum and Sanger chromatograms. **C.** NK cell cytotoxicity assays using KIL C.2 cells (Scramble or SHIP1-KO) against Vk*MYC targets (WT, CD48KO, CD48OE). Percent lysis is plotted across E:T ratios.

Supplementary Figure S7



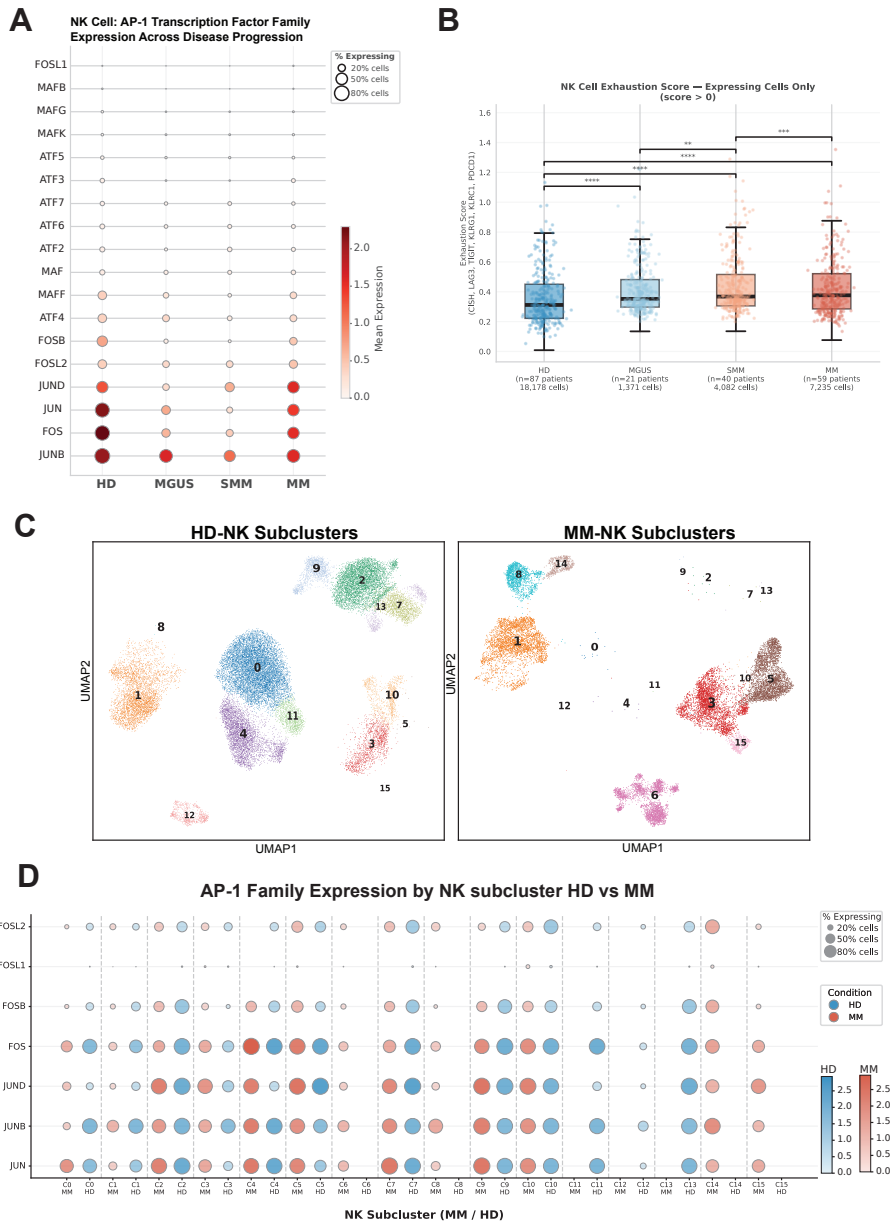
Supplemental Figure 7. Signaling Landscape and "CMV adaptive-like" CD56–dim phenotype Signatures in NK Cells from HD vs MM. A. CellChat analysis showing outgoing and incoming signaling patterns across immune subsets from healthy donor (HD) bone marrow. **B.** Violin plots comparing expression of "CMV adaptive-like" CD56–dim phenotype markers (FCER1G, KLRB1, KLRF1, KLRC2, KLRC3) in HD-NK vs MM-NK cells; p-values by Wilcoxon test. **C.** BATF expression HD-NK and MM-NK cells. **D.** Violin plot showing no significant difference in HLA-independent inhibitory receptors score between HD-NK and MM-NK cells and **E.** Violin plot showing CD48 expression in HD-NK and MM-NK. **F.** Heatmap displaying cluster-specific marker gene expression across NK-cell subclusters.

Supplementary Figure S8



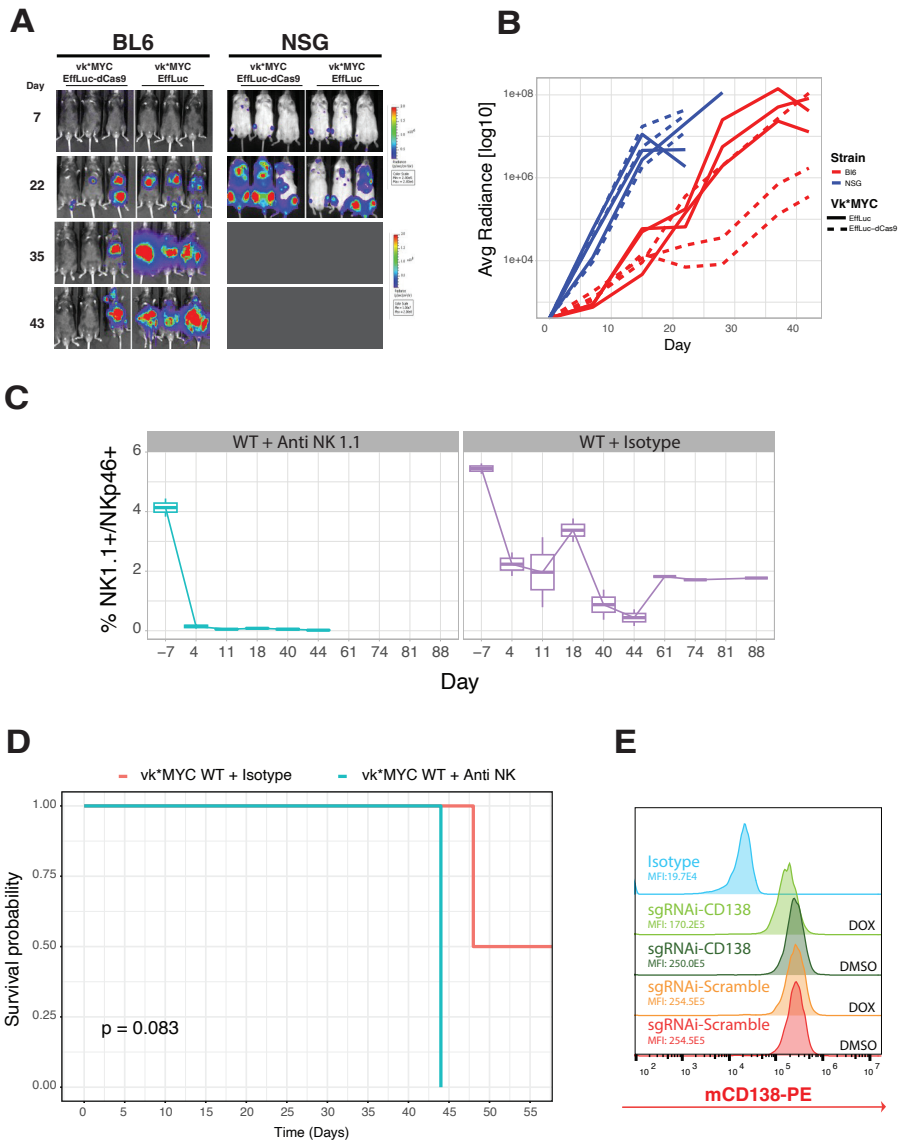
Supplemental Figure 8. NK-cell Exhaustion, CD56 expression, and AP-1 transcriptional profiles across NK-cell subclusters. A. FeaturePlot of NK-cell exhaustion module score (LAG3, TIGIT, KLRG1, KLRC1, CISH; calculated using Seurat AddModuleScore()) overlaid on the NK-cell UMAP, split by HD and MM. **B.** Violin plots of exhaustion module scores per NK subcluster (clusters 0–12), split by HD (salmon) and MM (teal). **C.** Scatter plot showing the correlation between NCAM1 mRNA expression (transcriptomic proxy for CD56) and exhaustion module score in HD and MM NK cells. **D.** DotPlot showing expression of AP-1 transcription factor family members (FOS, JUN, JUNB, FOSB, FOSL2) across NK-cell subclusters (0–12), split by Multiple Myeloma (MM, red) and Healthy Donor (HD, blue). Dot size reflects the percentage of cells expressing each gene per condition; color intensity reflects average expression level.

Supplementary Figure S9

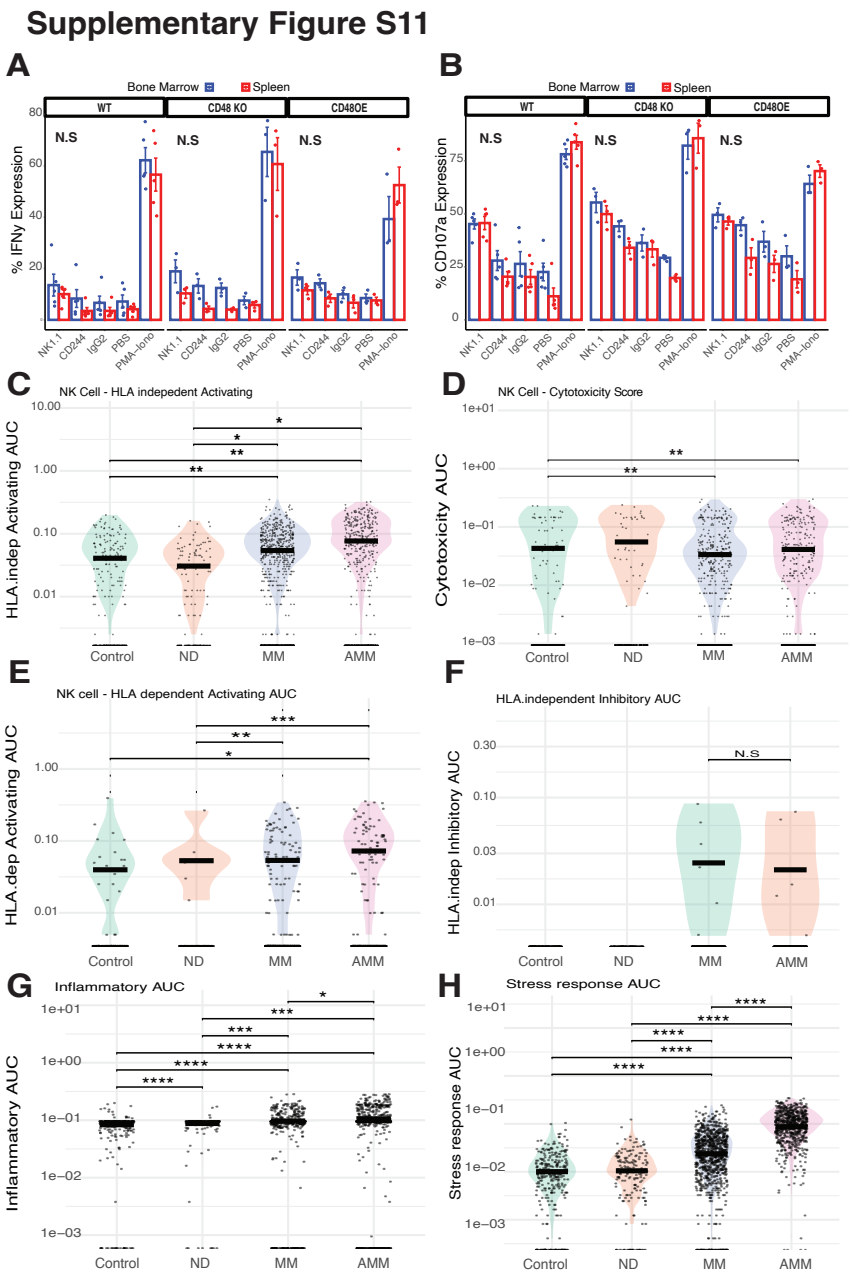


Supplemental Figure 9. AP-1 gene signature and NK exhaustion score across myeloma disease stages and NK subcluster-level AP-1 analysis in HD vs MM. A. DotPlot showing expression of AP-1 transcription factor family members across NK cells from HD, MGUS, SMM, and MM patients. Dot size reflects the percentage of cells expressing each gene; color intensity reflects mean expression level. **B.** Boxplot showing the NK cell exhaustion module score among NK cells expressing at least one exhaustion gene (score > 0), stratified by disease stage; pairwise comparisons performed using Mann-Whitney U test with Benjamini-Hochberg correction. **C.** NK cells from HD and MM patients were subclustered de novo using leiden clustering (resolution=0.5), identifying 16 transcriptionally distinct subpopulations. UMAP projections are shown separately for HD (left; n=86 patients, 29,966 cells) and MM (right; n=57 patients, 14,874 cells). Cluster labels are shown on data. **D.** DotPlot showing expression of AP-1 transcription factor family members across NK subclusters (C0–C15), split by HD (blue) and MM (red). Dot size reflects the percentage of cells expressing each gene; color intensity reflects mean expression level.

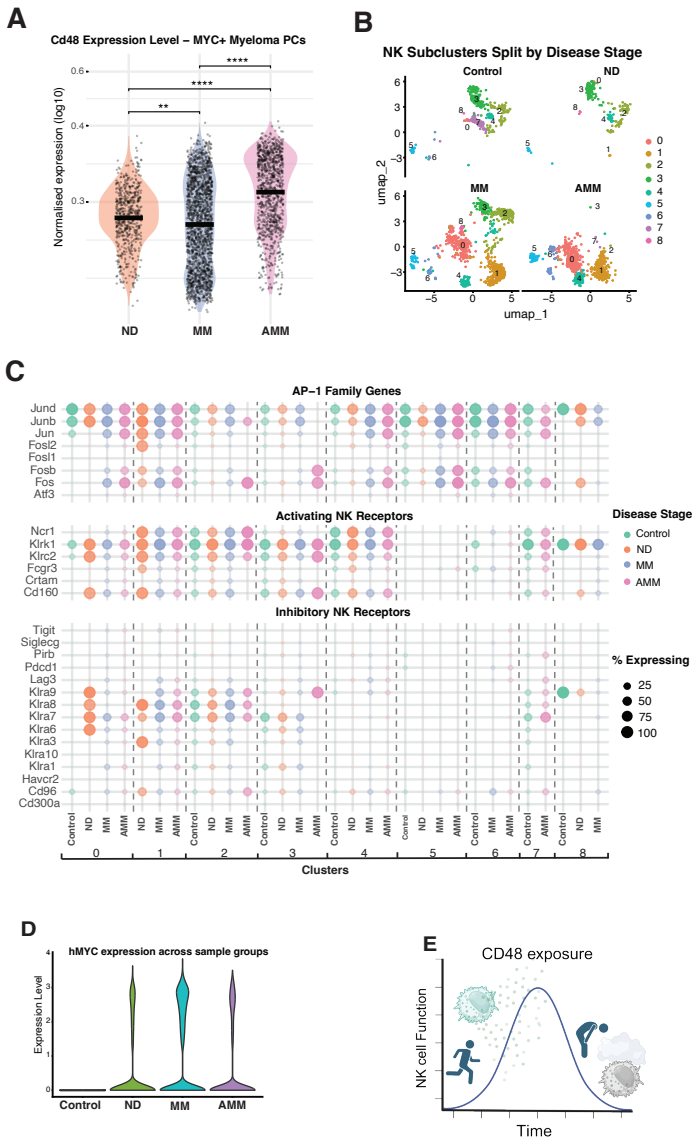
Supplementary Figure S10



Supplemental Figure 10. In Vivo Modeling of CD48 Function Using the Vk*MYC Luciferase and dCas9-KRAB System. A. Representative in vivo bioluminescent images of VkMYC-bearing BL6 and NSG mice. Tumor cells expressing firefly luciferase and/or dCas9-KRAB demonstrate successful engraftment and allow for tumor tracking without the need for serum protein electrophoresis (SPEP), in a non-secretory Vk*MYC clones (Vk32245). **B.** Longitudinal quantification of average tumor radiance (log10 scale) in each condition, grouped by mouse strain and tumor modification. **C.** Flow cytometry quantification of $NK1.1^{+}NKp46^{+}$ NK cells over time, comparing NK cell depletion (anti-NK1.1) versus isotype control in Vk*MYC WT. **D.** Kaplan–Meier survival curves comparing Vk*MYC WT mice with NK cell depletion versus isotype control. Statistical significance was assessed using the log-rank test. **E.** Flow cytometry analysis of CD138 expression in Vk*MYC cells engineered with a doxycycline-inducible sgRNA in a dCas9-KRAB constitutive system targeting CD138 (sgRNA-CD138), compared to scramble sgRNA control.



Supplemental Figure 11. NK Cell Functional Output and Transcriptional Programs in the Vk*MYC Mouse Model. A. Percentage of IFN-γ–producing NK cells in the bone marrow (blue) and spleen (red) of mice bearing WT, CD48KO, or CD48OE Vk*MYC tumors following ex vivo stimulation with anti-NK1.1, CD244, or PMA/ionomycin. No significant differences (N.S.) were observed across tissues. **B.** Percentage of CD107a⁺ degranulating NK cells under the same conditions as in panel A. CD48 manipulation did not significantly affect NK cell degranulation in either compartment. **C.** AUCell-based HLA-independent NK cell activation scores derived from single-cell RNA-seq data of tumor-infiltrating NK cells in Control, newly diagnosed (ND), multiple myeloma (MM), and advanced MM (AMM) samples from the immunocompetent Vk*MYC model. **D.** AUCell-based NK cell cytotoxicity scores **E.** HLA-dependent activating receptor score. **F.** HLA-independent inhibitory receptor score. **G.** Inflammatory Score. **H.** Stress response score. Individual data points represent single NK cells; horizontal lines indicate medians. P-values shown above brackets were calculated using Wilcoxon test with Benjamini-Hochberg correction. Statistical significance was determined using the Wilcoxon rank-sum test; *p < 0.05, **p < 0.01.



Supplemental Figure 12. Cd48 expression levels in MYC+ myeloma plasma cells across disease stages and NK-cell subclustering and receptor expression analysis in the de novo Vk*MYC model. **A.** Violin plot showing normalized Cd48 expression in MYC+ myeloma plasma cells from newly diagnosed (ND), established myeloma (MM), and advanced disease (AMM) mice. Only Cd48-expressing cells are shown (zero-expressing cells excluded). Horizontal lines indicate medians. Pairwise comparisons performed using Wilcoxon test with Benjamini-Hochberg correction. **p<0.01, ****p<0.0001. **B.** UMAP of de novo NK cell subclusters (clusters 0–8) identified by Seurat graph-based clustering via FindClusters (resolution=0.4), colored by subcluster identity (left) and disease stage (right). **C.** DotPlot showing AP-1 family gene expression (top), activating NK receptor expression (middle), and inhibitory NK receptor expression (bottom) across NK subclusters stratified by disease stage. Each column represents a subcluster-disease stage combination. Dot size reflects the percentage of cells expressing each gene; color reflects disease stage (Control: green; ND: orange; MM: blue; AMM: pink); color intensity reflects mean expression level. **D.** Violin plots of human MYC expression across four groups. **E.** CD48 exposure initially enhances NK-cell effector signaling/cytokine production but high CD48 cannot prevent longer-term exhaustion.

Feature	P_value	Significance	Enriched Cluster
CCND1	0.000376	***	A
Relapsed	0.00129	**	A
Gain1q21	0.00462	**	A
NSD2	0.0167	*	A
MAF	0.0301	*	B
Del1p22	0.134	n.s	A
Del17p13	0.161	n.s	A
MYC	0.272	n.s	A
MAFB	0.536	n.s	A

Supplemental Table 1. Genomic and Clinical Features Enriched in Transcriptomic Clusters Based on NK Cell Ligand Expression in Tumor Cells from Myeloma Patients (CoMMpass IA19 Bulk RNA-seq Dataset)

TF name	Cell name	GEO accession number	Description
MEF2B	GM12878	GSE127481	B-lymphocyte, lymphoblastoid, normal
MEF2C	GM12878	GSE32465	B-lymphocyte, lymphoblastoid, normal
RELA	GM12878	GSE31477/GSM935478	RELA ChIP-seq on human GM12878 treated with TNFa for 6h
RELA	GM10847	GSE31477/GSM935527	Lymphoblastoid, International HapMap Project, CEPH/Utah, treatment: Epstein-Barr Virus transformed
RELA	GM12891	GSE31477/GSM935526	B-lymphocyte, lymphoblastoid, International HapMap Project, CEPH/Utah pedigree 1463, treatment: Epstein-Barr Virus transformed
RELA	GM12892	GSE31477/GSM935285	B-lymphocyte, lymphoblastoid, International HapMap Project, CEPH/Utah pedigree 1463, treatment: Epstein-Barr Virus transformed
RELA	GM15510	GSE31477/GSM935529	Lymphoblastoid NIGMS Human Genetic Cell Repository, DNA Polymorphism Discovery Resource Collection, treatment: Epstein-Barr Virus transformed
RELA	GM18505	GSE31477/GSM935282	Lymphoblastoid, International HapMap Project, Yoruba in Ibadan, Nigera, treatment: Epstein-Barr Virus transformed
RELA	GM18526	GSE31477/GSM935281	Lymphoblastoid, International HapMap Project, Han Chinese in Beijing, China, treatment: Epstein-Barr Virus transformed
RELA	GM18951	GSE31477/GSM935531	Lymphoblastoid, International HapMap Project, Japanese in Tokyo, Japan, treatment: Epstein-Barr Virus transformed
RELA	GM19099	GSE31477/GSM935273	Lymphoblastoid, International HapMap Project, Yoruba in Ibadan, Nigera, treatment: Epstein-Barr Virus transformed
RELA	GM19193	GSE31477/GSM935279	Lymphoblastoid, International HapMap Project, Yoruba in Ibadan, Nigera, treatment: Epstein-Barr Virus transformed
TFAP2A	HeLa-S3	GSE31477/GSM935367	Cervical carcinoma, cancer
ESRRA	GM12878	GSE31477/GSM1003605	B-lymphocyte, lymphoblastoid, normal
ESRRA	HepG2	GSE31477/GSM935621	Homo sapiens HepG2 treated with 1 mM pyruvate for 6 hours, 1 µM forskolin for 6 hours
ESRRA	K562	GSE91805	Leukemia, cancer
ESRRA	MCF-7	GSE92187	Mammary gland, adenocarcinoma. Breast cancer
ESRRA	A549	GSE91793	Lung cancer
TFAP2A	HCT116	GSE155165/GSM4696472	Parental cell line, Clone 24 and 120 with CRISPR/Cas9 KO of AP-2a.
RELA	HeLa	GSE116284	Cervical carcinoma. WT cell line and RELA siRNA-mediated p65/RELA knockdown reconstituted with WT, DNA-binding (E39I), or transactivation-deficient (FLDD) p65 mutants, with or without TNF-α stimulation (0h and 1h).

***Supplementary Table S2**. Public ChIP-seq datasets used to assess transcription factor occupancy at the CD48 locus across hematopoietic and non-hematopoietic cell types.*